CHEMISTRY OF MATERIALS

Article

Influence of Terminal Carboxyl Group on Structure and Reactivity of Functionalized m-Carboranethiolate Self-Assembled Monolayers

Dominic P Goronzy, Jan Stanek, Erin Avery, Han Guo, Zdenek Bastl, Michal Dusek, Nathan M. Gallup, Saliha Gün, Monika Ku#eráková, Brian J. Levandowski, Jan Machacek, Václav Šícha, John C Thomas, Adem Yavuz, K. N. Houk, Mehmet Fatih Dani#man, Ersen Mete, Anastassia N. Alexandrova, Tomas Base, and Paul S. Weiss

Chem. Mater., **Just Accepted Manuscript** • DOI: 10.1021/acs.chemmater.0c02722 • Publication Date (Web): 10 Jul 2020

Influence of Terminal Carboxyl Group on Structure and Reactivity of Functionalized *m*-Carboranethiolate Self-Assembled Monolayers

Dominic P. Goronzy,[1,2] Jan Staněk,[3] Erin Avery,[1,2] Han Guo,[1] Zdeněk Bastl,[4] Michal Dušek,[5] Nathan M. Gallup,[1] Saliha Gün,[6] Monika Kučeráková,[5] Brian J. Levandowski,[1] Jan Macháček,[3] Václav Šícha,[3,7] John C. Thomas,[1,2] Adem Yavuz,[8] K. N. Houk,[1*] Mehmet Fatih Danışman,[6,8*] Ersen Mete,[9*] Anastassia N. Alexandrova,[1*] Tomáš Baše,[1,2,3*] and Paul S. Weiss[1,2,10,11*]

[1]Department of Chemistry and Biochemistry, University of California, Los Angeles, Los Angeles, California 90095, United States

[2]California NanoSystems Institute, University of California, Los Angeles, Los Angeles, California 90095, United States

[3]The Czech Academy of Sciences, Institute of Inorganic Chemistry, 250 68 Husinec-Řež, č.p. 1001, Czech Republic

[4]The Czech Academy of Sciences, J. Heyrovský Institute of Physical Chemistry, Dolejškova 3, 182 23 Prague 8, Czech Republic

[5]The Czech Academy of Sciences, Institute of Physics, Na Slovance 1999/2, 182 21 Prague 8, Czech Republic

[6]Department of Chemistry, Middle East Technical University, Ankara 06800, Turkey

[7]Department of Chemistry, Faculty of Science, Jan Evangelista Purkyne University in Usti nad Labem, Czech Republic

[8]Micro and Nanotechnology Department, Middle East Technical University, Ankara 06800, Turkey

[9] Department of Physics, Balikesir University, Balikesir 10145, Turkey

[10]Department of Bioengineering, University of California, Los Angeles, Los Angeles, California 90095, United States

[11]Department of Materials Science and Engineering, University of California, Los Angeles, Los Angeles, California 90095, United States

ABSTRACT

The structure and function of self-assembled monolayers (SAMs) at the nanoscale are determined by the steric and electronic effects of their building blocks. Carboranethiol molecules form pristine monolayers that provide tunable two-dimensional systems to probe lateral and interfacial interactions. Additional ω-functionality, such as carboxyl groups, can be introduced to change the properties of the exposed surfaces. Here, two geometrically similar isomeric *m*-carborane analogs of *m*-mercaptobenzoic acid, 1-COOH-7-SH-1,7-$C_2B_{10}H_{10}$ and *racem*-1-COOH-9-SH-1,7-$C_2B_{10}H_{10}$, are characterized and their SAMs on Au{111} are examined. The latter isomer belongs to the rare group of *chiral* cage molecules and becomes, to our knowledge, the first example assembled on Au{111}. Although different in symmetry, molecules of both isomers assemble into similar hexagonal surface patterns. The nearest neighbor spacing of 8.4 ± 0.4 Å is larger than that of non-carboxylated isomers, consistent with the increased steric demands of the carboxyl groups. Computational modeling reproduced this spacing and suggests a tilt relative to the surface normal. However, tilt domains are *not* observed experimentally, suggesting the presence of strong lateral interactions. Analyses of the influence of the functional groups through the *pseudo*-aromatic *m*-carborane skeleton showed that the thiol group attached to either carbon or boron atoms increases the carboxyl group acidity in solution. In contrast,

the acidity of the exposed carboxyl group in the SAMs *decreases* upon surface attachment; computational analyses suggest that the driving force of this shift is the dielectric of the environment in the monolayer as a result of confined intermolecular interactions, proximity to the Au surface, and partial desolvation.

INTRODUCTION

Two-dimensional self-assembled materials, in addition to their utility for numerous applications, are important tools in advancing our understanding of the principles of self-assembly.[1-4] As such, developing building blocks is of fundamental importance in enabling the investigation of specific steric and electronic effects or intermolecular interactions within self-assembled monolayers (SAMs).[5] Organic molecules have been extensively explored in this field, offering possible analogies to naturally occurring biological systems and allowing studies of the impact of defined chemical modifications.[2] Introduction of additional ω-functionality such as carboxyl groups resulted in different properties of the surfaces, determined by hydrogen-bonding intermolecular interactions and hydrophilicity.[6-8] Several systems, including carboxyl-terminated alkanethiols and mercaptobenzoic acids, have been investigated as convenient building blocks on both flat and colloidal surfaces.[9-11] In these particular systems, the anchoring thiol and the exposed carboxyl groups are separated by either conformationally flexible aliphatic -$(CH_2)_x$- alkyl chains or sheet-like aromatic -(C_6H_4)- benzene rings with different steric requirements and mutual interactions.

In our laboratories, we have introduced carborane building blocks that, due to symmetry, have lower total numbers and fewer defects within their molecular monolayers compared to organic systems.[5,12,13] These differences are at least partly due to their rigid

molecular architectures with lower conformational freedom. Carborane–based systems enable us to obtain surface assemblies of different isomers in identical or highly similar surface patterns. The *para*-carboranethiol cage analogue of *para*-mercaptobenzoic acid has been shown to assemble into a hexagonal pattern identical to that of its non-carboxylated parent analogue, with no influence of the carboxyl group on the nearest neighbor spacing.[11] The closest hexagonal packing of carboranethiol molecules on flat surfaces simply compares to the tightest filling of the surface by solid spheres, *i.e.*, the projection of the cage onto the surface, similar to previously observed behavior of other architecturally rigid bulk molecules such as adamantane derivatives.[14-16] The structurally rigid bodies of carboranes enable unprecedented variability of isomeric structures whilst the surface lattice remains either the same or is only gently modified.[5,17-20] In this regard, special attention has been paid to the dipole moment orientation, which is mainly given by the positioning of the carbon atoms in the cage, and to its effect on work function changes.[21-25]

Building on these advances, we prepared two isomeric bifunctional cage molecules based on the *meta*-carborane skeleton, juxtaposing them to their organic analogue, *meta*-mercaptobenzoic acid, as well as the previously studied *para*-isomer as building blocks for SAMs. Both new isomers show practically identical orientations of functional groups with respect to the centroid of the *meta*-carborane cage but differ in chemical and physical properties as determined by the electron-donating and withdrawing properties of the molecular cage scaffold. In addition, they differ in their symmetry; one of them belonging to a rather rarely investigated group of chiral cage borane derivatives.[26] Assemblies of chiral molecules on surfaces are currently of interest due to their spin-filtering effects in electron transport.[27-30]

The interactions of both functional groups, interspaced by the *meta*-carborane skeleton, were analyzed in SAMs *vis-à-vis* the differences of the two isomers. Furthermore, the effect of increased lateral interactions on the assembly of these monolayers was experimentally examined and the results were compared to computational models. Lastly, the change in behavior of the carboxyl functional group was probed, as it moves from an unrestricted three-dimensional environment to the exposed interface of a surface-bound two-dimensional array.

Materials and Methods

A detailed description of materials and methods is provided in the Supporting Information. Briefly, self-assembled monolayer samples were prepared on Au{111}/mica substrates, Au/Cr/Si substrates, and template-stripped Au chip substrates for scanning tunneling microscopy imaging (STM), contact angle measurements, and X-ray photoelectron spectroscopy (XPS) experiments, respectively. For deposition, substrates were immersed in ethanoic solutions of 1-4 mM concentration for up to 24 h. A custom-built Besocke-style scanning tunneling microscope was used for STM measurements and imaging was performed under ambient conditions. Contact angle measurements were taken on a FTA1000 drop shape instrument contact angle goniometer. For contact angle titrations, the contact angle measurements were performed using a series of buffers ranging from pH 2 to 12. For XPS measurements, monolayers were subsequently modified by immersion in aqueous metal ion salt solutions or aqueous HCl solution. These measurements were performed on a Kratos Axis Supra XPS instrument.

RESULTS AND DISCUSSION

Intrinsic properties and characteristics of carboxylated *meta*-carboranes

Isomeric bifunctional carborane species were synthesized from the respective thiol derivatives of *meta*-carborane by their lithiation and subsequent reaction with CO_2 followed by acidic hydrolytic quenching: 1-SH-1,7-$C_2B_{10}H_{11}$ (**M1**) produced 1-COOH-7-SH-1,7-$C_2B_{10}H_{10}$ (**M1-COOH**) and 9-SH-1,7-$C_2B_{10}H_{11}$ (**M9**) was transformed into *racem*-1-COOH-9-SH-1,7-$C_2B_{10}H_{10}$ (**M9-COOH**). Detailed procedures and a schematic representation are available in the supporting information (Scheme S1). X-ray diffraction studies confirmed that the two isomers have nearly identical geometries with the angle $\alpha[C_{COOH}$, centroid, $S_{SH}]$ of 114.54° in **M1-COOH** and 115.31° in **M9-COOH**. Figure 1 shows the crystallographically determined structures of these two isomers. Computationally optimized geometries, also shown in Figure 1, were consistent with experimental data and include the projections of the orientations and the relative strengths of the dipole moments. Both isomeric molecules exhibit different molecular symmetries due to the specific positioning of functional groups on the *meta*-carborane cluster core, which are reflected in their ^{11}B and ^{1}H NMR spectra (Figures S1-S5, Tables S1-S3). For both of these isomers the carboxyl group is attached to an electron-accepting carbon vertex; the thiol functional group in **M1-COOH** is also attached to an electron-accepting carbon vertex, in contrast to an electron-donating boron vertex in **M9-COOH**. The **M9-COOH** isomer is chiral with both enantiomers resolved in a racemic single-crystal structure analyzed by X-ray diffraction (Figures S6-S8, Tables S4 and S5). The two isomers exhibit similar intermolecular hydrogen interactions in their supramolecular crystal structures, dominated by the carboxyl and thiol functional groups. Additionally, the two molecules

showed similar isotopic distributions in their ESI mass spectra and were further characterized by infrared spectroscopy (Figures S9-S20).

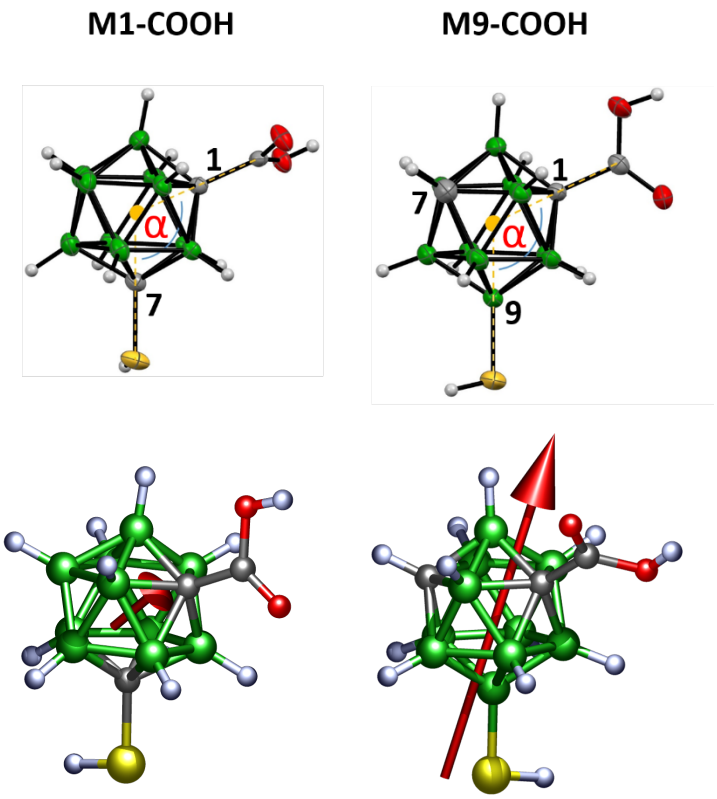

Figure 1. Structures of carboxylated *meta*-carboranethiol isomers. Crystallographically determined molecular structures of **M1-COOH** and **M9-COOH** with 50% probability ellipsoids for the non-hydrogen atoms (upper panel). The lower schematics of both isomers show computationally optimized structures with arrows indicating the orientations and the relative magnitudes of the dipole moments, 0.57 D for **M1-COOH** and 2.58 D for **M9-COOH**. The yellow dots in the crystallographically determined structures represent the centroids of the C_2B_{10} cage parts of the molecules. Boron atoms are shown in green, carbon atoms are shown in gray, oxygen atoms are shown in red, sulfur atoms are shown in yellow, and hydrogen atoms are shown in white.

The differences between the effects of the electron-accepting carbon and the electron-donating boron vertices on the thiol group are consistent with previous studies, which relate the thiol group character to the type of the carborane skeleton (*ortho*-, *meta*-, or *para*-) and to the thiol group's position on the cage.[31-34] The new bifunctional molecular system with one carboxyl group and one thiol group enabled us to investigate their mutual influence on their positions on the *meta*-carborane cage. In the case of **M1-COOH**, both functional groups are attached to the carbon atoms, the electron-withdrawing vertices of the *meta*-carborane scaffold. In the isomer **M9-COOH**, the thiol group is attached to a boron atom, through which *meta*-carborane manifests a relatively strong electron-donating effect. Table 1 provides a summary of selected characteristic parameters related to the chemical nature of the functional groups; these properties are important for their intramolecular communication, as well as for their roles in self-assembly, as discussed below. The ^{1}H NMR shifts of the respective thiol groups and the carboxyl pK_a values of both isomers are displayed in Table 1 (See also Tables S1 and S2 and Figures S4 and S21). For comparison, the pK_a value of the *meta*-carborane-1-carboxylic acid (**M-COOH**) is also reported. Both **M1** and **M1-COOH** show practically the same values of ^{1}H NMR shift of their thiol groups, at *ca*. 3.4 - 3.5 ppm. In comparison, the ^{1}H NMR shifts of the thiol groups in both **M9** and **M9-COOH** are lower, at about 0.5 ppm, which is in accord with the electron-donating character of the boron vertex of *meta*-carborane. Note that the thiol chemical shifts in the ^{1}H NMR spectrum not only manifest the electron-accepting (as in **M1** or **M1-COOH**) and electron-donating (as in **M9** and **M9-COOH**) effects of the *m*-carboranyl cage moiety but also show, consistent with our previous findings, that the carboxyl group does not significantly influence the thiol group in this regard. By contrast,

the thiol group interacts significantly with the molecular skeleton and thus increases the carboxyl group acidity as evident from the lower pK_a values in both isomers compared to **M-COOH** (1-COOH-*m*-$C_2B_{10}H_{11}$) (For characterization data on this molecule see Figures S5, S17, and S20 and Table S3).

Table 1. Experimental ^{1}H NMR chemical shifts of the thiol (SH) groups and the carboxyl (COOH) pK_a values of the new isomeric derivatives and their parent compounds.

Derivative	^{1}H NMR (SH)	pK_a (COOH)
M1	3.39	–
M1-COOH	3.46	3.01
M9	0.47	–
M9–COOH	0.52	3.23
M–COOH	–	3.76

Characterization of Self-Assembled Monolayers *via* Scanning Tunneling Microscopy

Scanning tunneling microscopy (STM) was used to image homogeneous SAMs of both **M1-COOH** and **M9-COOH** on Au{111}/mica with molecular resolution under ambient conditions. Both isomers form into hexagonal close-packed structures with nearest-neighbor distances of 8.4 ± 0.4 Å (Figures 2 and S22). These results are remarkable

given that in the previous study of the *para*-isomer, molecularly resolved images of the homogeneous carboxylic-acid terminated monolayer were unattainable.[11] We hypothesize that the orientation of the carboxyl group directly into the environmental interface in the case of the *para* isomer results in greater conformational freedom and greater interaction with ambient water, which thereby leads to a lack of molecular resolution. Additionally, the attachment of a carboxyl group to the parent molecules, **M1** and **M9**, increases the steric demands of both isomeric molecules as compared with the lateral steric requirements of the parent non-carboxylated derivatives, which both have nearest-neighbor distances of 7.2 ± 0.4 Å.[12] The molecular symmetry differences between the isomers have no direct influence on the geometry of the surface lattice, as evidenced by isostructural monolayers with experimentally indistinguishable nearest neighbor spacings. Two phases were observed in the monolayers, which differed in apparent height by 1.0 ± 0.3 Å in both **M1-COOH** and **M9-COOH** SAMs. The higher apparent protrusion is the minority phase with coverage of 3 ± 1% in SAMs of both isomers (Figure S23). This feature has been observed previously and attributed to a mixture of thiolate- and thiol-bound moieties, with the latter being the more protruding apparent height feature in STM images.[11] Alternatively, the carboxylic acid may have partially converted to an ester in the molecules in the minority phase, as the relative population size of the phase is consistent with spontaneous esterification. We also observed rotational domains in the monolayers and, as has been reported previously for other carboranethiol SAMs, these domains did not have prominent domain boundaries in STM images.[12]

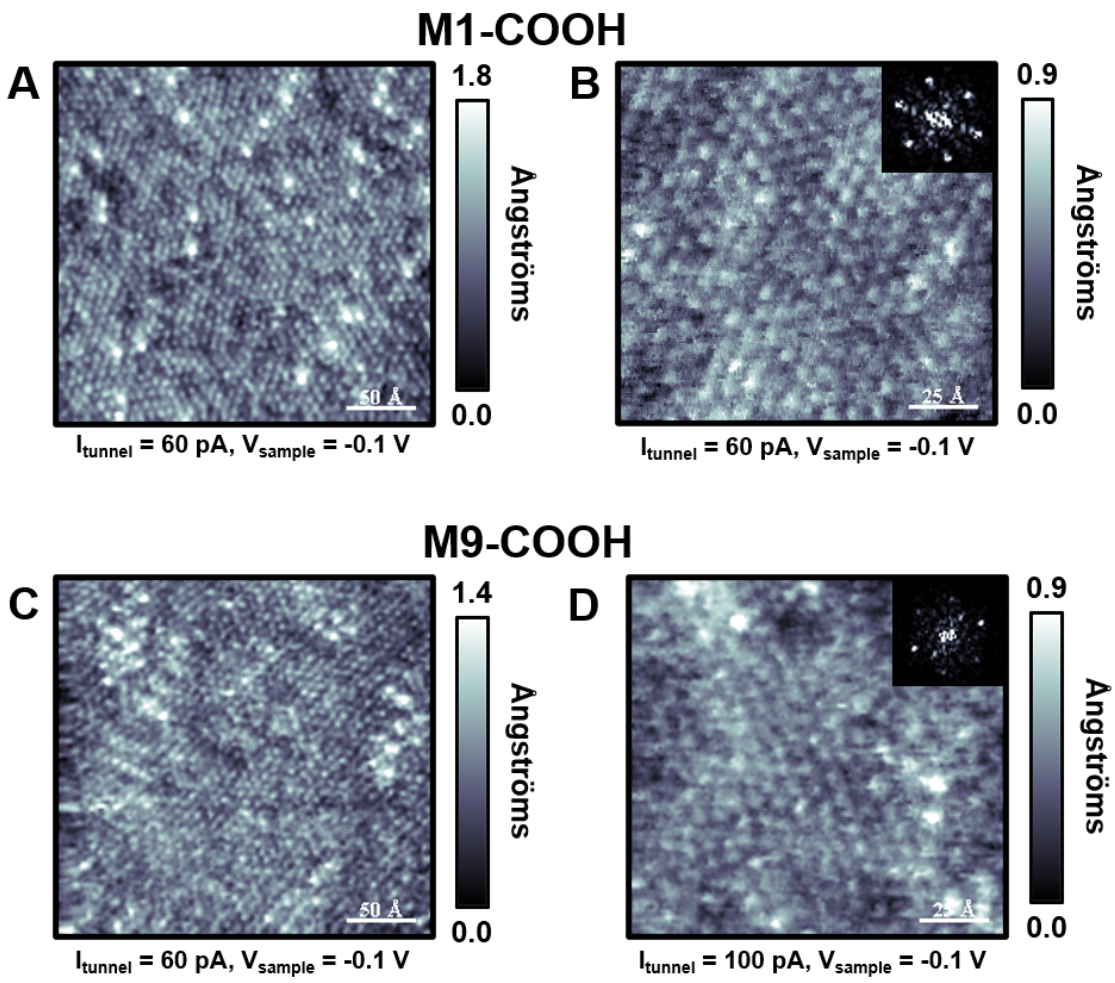

Figure 2. Scanning tunneling microscopy images of (A,B) **M1-COOH** and (C,D) **M9-COOH** self-assembled on Au{111}. All images were taken at ambient conditions. Insets depicting Fourier transforms of (B) and (D) show hexagonal close-packed arrays with identical nearest-neighbor distances of 8.4 ± 0.4 Å for both isomers.

The possible unit cells that are commensurate with the unreconstructed Au{111} substrate are (5 × 5) and (3 × 3), have nearest–neighbor distances of 8.3 Å and 8.64 Å, respectively, with reference to the 2.88 Å lattice constant of the substrate surface. Both are within experimental error of the determined values. The (3 × 3) unit cell consists of one

SAM molecule binding with its sulfur atom to a two-fold bridge site, while the (5 × 5) unit cell consists of three SAM molecules binding atop and three-fold hollow sites in a 1:2 ratio.

Computational Analysis of the Self-Assembled Monolayer Structure

As determined by the STM analysis, the presence of a carboxyl functional group increases the steric demands of the molecules within the SAM. To explore these lateral interactions further, we performed several computational analyses. In examining the space-filling model from projection onto the surface, we find that a molecular tilt of 13-16° minimizes the projection area and therefore maximizes the packing density. This minimum corresponds to a nearest-neighbor distance of 8.6 Å, which is in close agreement with what we observed experimentally with STM (Figure 3).

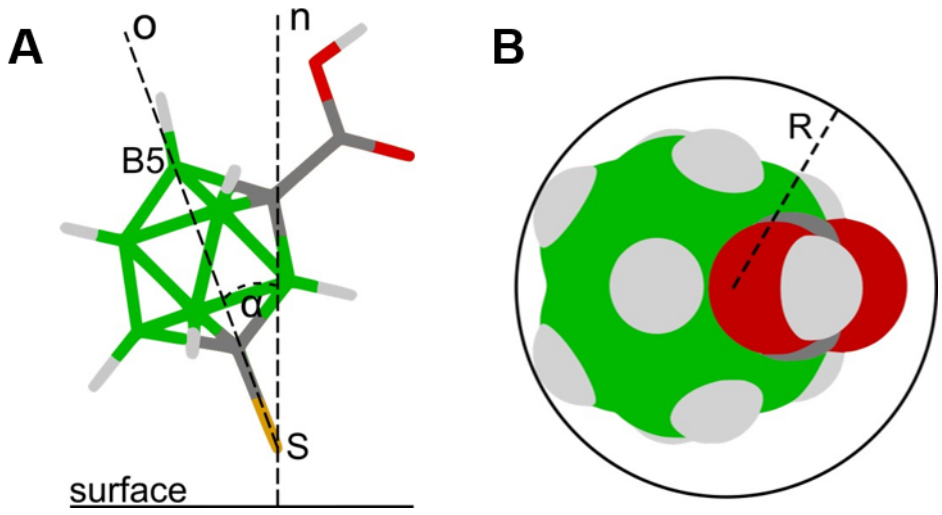

Figure 3. (A) Schematic representation of the isomeric molecule **M1-COOH** tilted 13-16° (α) from the surface normal and (B) the respective space-filling model projection onto the surface (R=8.6 Å).

Although this geometric, space-filling model is highly intuitive and the nearest-neighbor distance derived from it corresponds well to the experimental data, it also requires assumptions about the rigidity of the molecule, such as the static axis intersecting the sulfur atom and the antipodal boron vertex. We performed density functional theory (DFT) calculations using the SCAN-rVV10 functional for both isomeric species to provide rigorous details about the molecular tilt on the surface. Both the (3 × 3) and (5 × 5) unit cells were examined, but only the (3 × 3) unit cell corresponds to a densely packed monolayer and thus provides a comparison to the acquired experimental data. The computationally calculated nearest-neighbor distance of the (5 × 5) unit cell was 13.72 Å, which deviated significantly from what was measured experimentally. The results of the (3 × 3) unit cell model are summarized in Table 2 and depicted in Figure 4. Optimized geometries revealed two different conformations (A and B), one of which shows the molecule tilted backwards to expose the carboxyl group to the monolayer-environment interface (A); the other conformation shows the molecule leaning with the carboxyl group towards the neighboring molecule and hydrogen bonding in the lateral direction (B). While the first conformation can be understood as a result of favorable steric preferences, the second conformation could result from favorable lateral interactions between the positively charged carboxyl proton and negatively charged cluster vertices of the adjacent molecule. Similar interactions between acidic hydrogen atoms and BH cluster vertices of the appropriate charge have been reported previously to occur in 3D single crystals.[35] The energy difference between geometries A and B is relatively small, ~1 $kJ \cdot mol^{-1}$ (Figure 4), and as a result the configurations are practically indistinguishable.

Computationally, **M1-COOH** is found to be stable in both conformations while **M9-COOH** is only stable in configuration B. However, we do *not* see evidence for the existence of two conformations in the STM data; we see neither a mixture of configurations A and B in SAMs of **M1-COOH** nor structural differences between the SAMs of the two isomers. It is possible that ambient STM cannot differentiate between the two configurations. Calculations show that the charge density that the STM probes is located mostly in the central cage of the molecule and, as such, the two configurations would look similar; this observation is further supported by simulated STM images (Figures S24 and S25). Thus, it is inconclusive whether both configurations occur in the SAMs simultaneously or only one configuration is present.

Moreover, as with many other cage-molecule SAMs, we do not observe the typical domain boundary defects that accompany molecular tilt, which the computational analysis predicts are required in order to achieve the experimentally observed packing density. One possible explanation for the absence of tilt defects is that long-range intermolecular interactions, which in the case of these molecules could be a combination of hydrogen-bonding and favorable dipole-dipole interactions, have azimuthally locked the molecules into one orientation. Note that only in configuration B, in which molecules lean on their neighbors and form rows, are hydrogen-bonding interactions possible and computationally predicted. Both hydrogen-bonding networks and dipole-dipole interactions have previously been shown to overcome structural domain boundaries in SAMs.[22,36] Additionally, given the propensity of carboxylic acids to form dimers, we modeled this interaction. The model predicted that this interaction is only stable with a significantly larger nearest neighbor spacing in a (6 × 3) unit cell (Figure S26). Given this

model and the fact that we do not see any evidence of dimers in the STM data, it is unlikely that they are present in the SAMs. Lastly, we note that the computational model does not incorporate adatoms in the computation; adatoms have previously been shown to significantly contribute to the structural characteristics of SAMs on gold surfaces.[37-39]

Table 2. Dissociative chemisorption energies, E_C (eV), and molecular tilt angles $\Theta_{S\text{-}Cage}$ (°) and Θ_{Cage} (°) schematically shown in Figure S27.

Configuration		E_C (eV)	$\Theta_{S\text{-}Cage}$ (°)	Θ_{Cage} (°)
M1-COOH	(3 × 3) A	-1.56	36.2	28.7
M1-COOH	(3 × 3) B	-1.57	21.6	16.7
M9-COOH	(3 × 3) B	-1.60	15.5	10.5

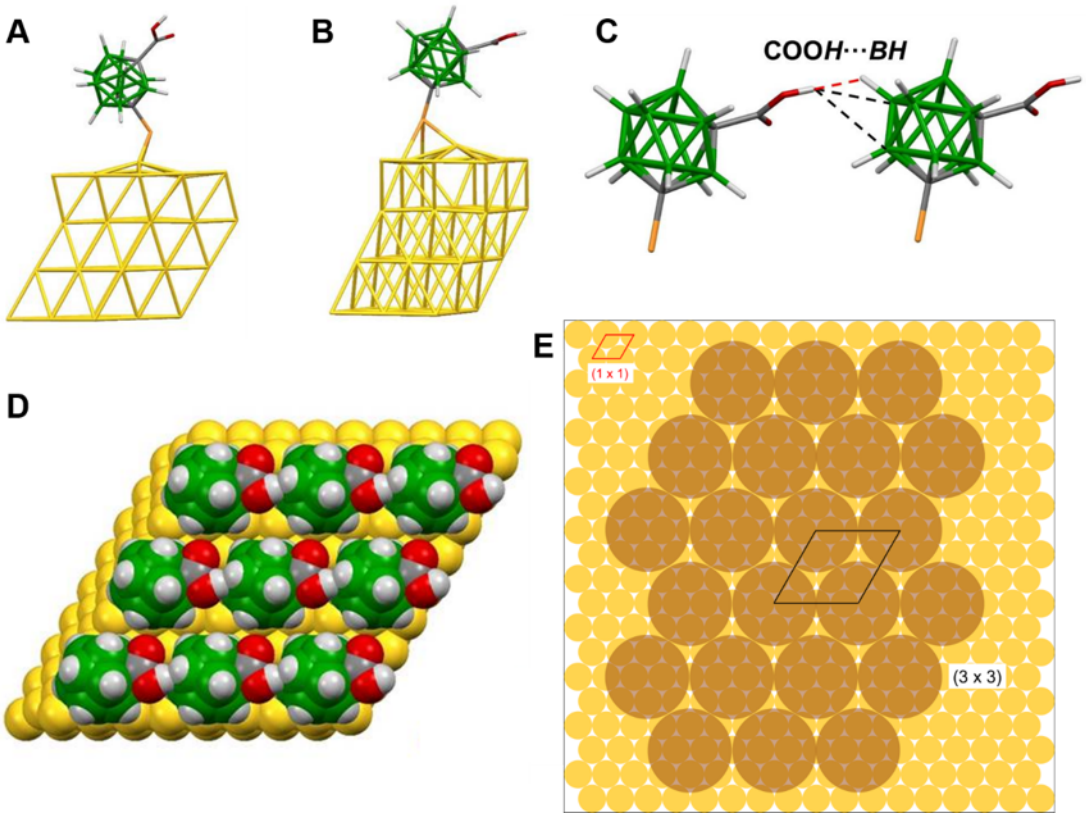

Figure 4. (A,B) Two stable calculated conformations of **M1-COOH**. (C) Schematic of calculated potential lateral hydrogen bonding of COOH—HB (red) and COOH—BH (black), with bond lengths of 1.826 Å and 2.833 Å, respectively. (D) Space-filling model and (E) schematic of a densely packed monolayer with a (3 × 3) unit cell with respect to the underlying gold.

Interactions with the Au{111} Substrate

The bonding of both isomeric molecules to gold surfaces was investigated by X-ray photoelectron spectroscopy (Table 3), which showed the molecules adsorb as thiolates. The measured atomic concentrations of boron and sulfur fitted the nominal stoichiometry of the molecules, $B_{10}S_1$. The measured binding energy values of S $2p_{3/2}$ electrons at 162.3 eV for **M1-COOH** and at 161.7 eV for **M9-COOH** indicated typical thiolate bonds. The

difference of ~0.6 eV between the isomers is consistent with the previously discussed electron-accepting and donating properties of the particular *meta*-carborane vertices in the SAM molecules. In **M9-COOH**, the *meta*-carboranyl moiety increases the electron density on the thiolate sulfur atoms, which leads to the lower binding energy value of the S $2p_{3/2}$ electrons compared to **M1-COOH**.

Table 3. Measured Core-Level Binding Energies and full width half maxima (in parentheses) for Au films modified with **M1**, **M9**, **M1-COOH**, **M9-COOH**.

Sample	S $2p_{3/2}$
M1	162.2 (0.8)
M1-COOH	162.3 (0.8)
M9	161.7 (0.8)
M9-COOH	161.7 (0.8)

Carboxylic Acid at the Exposed Interface

Anchoring the isomeric molecules to gold surfaces gives us the opportunity to probe the chemical character of the exposed carboxyl groups, which enables the SAMs to engage in further interactions and reactions. We have examined the carboxyl functional group by measuring dynamic contact angles (Table 4) and probed the accessibility for further chemical bonding with several ions. In both cases, the constituent makes the surface more hydrophilic compared to SAMs of their parent non-carboxylated derivatives **M1** and **M9**.

Table 4. Dynamic contact angles for parent **M1** and **M9** isomeric species, as reported in Ref. [12], and the respective carboxylated analogues **M1-COOH** and **M9-COOH** assembled on gold surfaces. (N = 8)

Sample	Θ_a	Θ_r
M1[12]	82 ± 2	71 ± 1
M9[12]	72 ± 4	52 ± 1
M1-COOH	61 ± 1	42 ± 1
M9-COOH	66 ± 1	55 ± 1

Θ_a: advancing contact angle, Θ_r: receding contact angle

To study the sensitivity of the carboxyl group to the attachment of a thiol group at either the second carbon or the boron atom of the *meta*-carborane skeleton, we analyzed the carboxyl group acidity of both isomers assembled on gold surfaces, *i.e.*, after the thiol group scission and thiolate-gold bond formation. We probed the acidity on the surface *via* contact angle titration.[40] In this titration, the advancing contact angle is measured over a range of pH points. A decrease in the contact angle signifies deprotonation as the newly formed ion increases the surface hydrophilicity. The midpoint between the protonated and deprotonated states can be defined as the apparent surface pK_a. To control for confounding factors of acidic pH on surface assemblies, we used starting pH between 2 and 4 in the titration experiments, with similar results. The results of the contact angle titration provided an apparent surface pK_a of 5.1 ± 0.6 and 4.8 ± 0.7 for **M1-COOH** and **M9-COOH**, respectively (Figure 5). By comparison, the control experiment **M9** SAM shows no change in contact angle as a function of pH (Figure S28). Thus, the pK_a shifts from solution to

surface by approximately two pH units for both isomers, consistent with previous observations with carboxyl-terminated monolayers.[40,41] The two isomers did not significantly differ in apparent surface pK_a although we may have missed smaller differences due to variability of measurements; controlling for several technical variables, including ambient humidity, batch-to-batch variation, and substrate fabrication did not reduce the measurement variability.

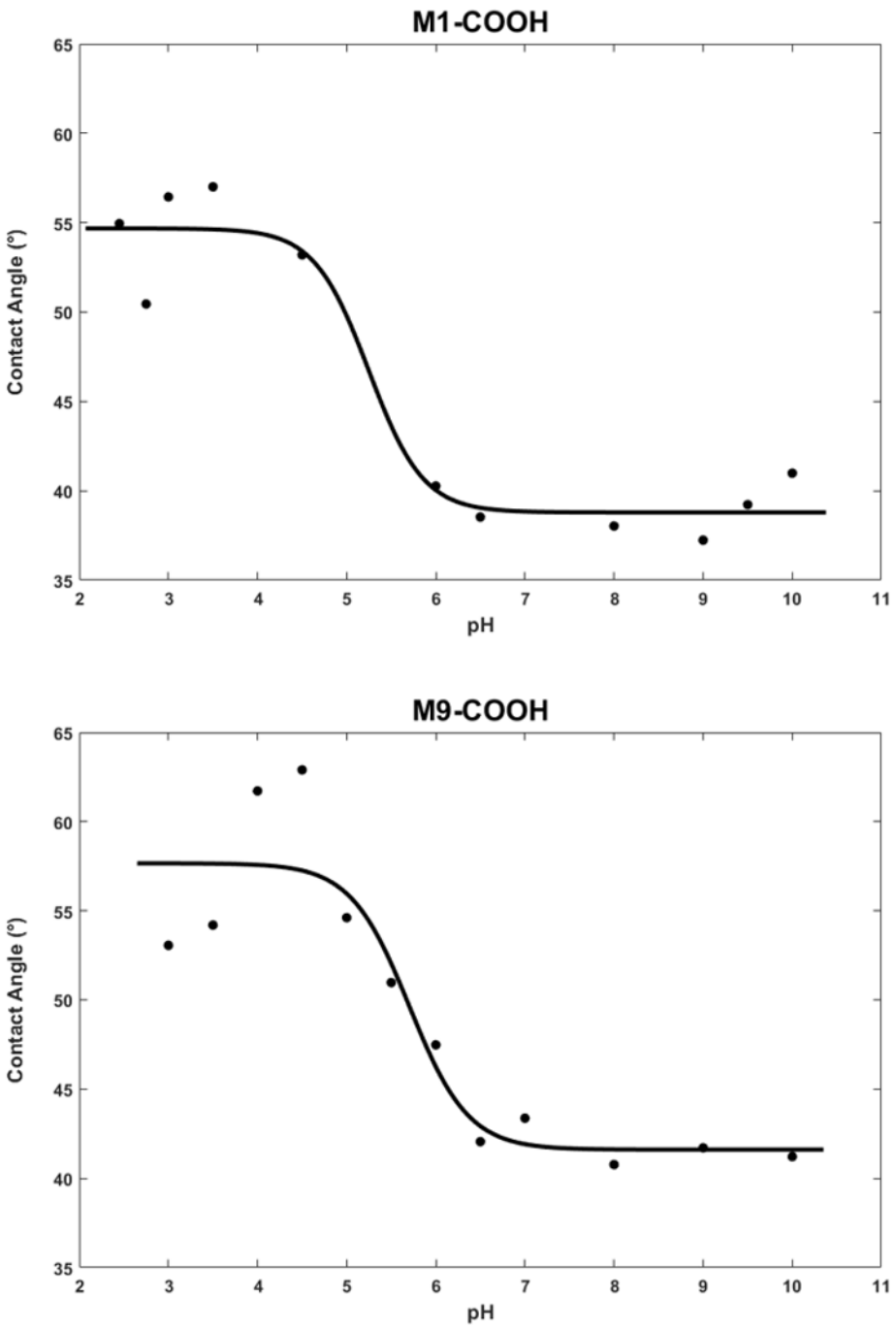

Figure 5. Representative contact angle titration curves for (top) **M1-COOH** and (bottom) **M9-COOH**. The surface pK_a for the two isomers are 5.1 ± 0.6 and 4.8 ± 0.7, respectively (N=5).

To understand the altered state of the carboxylic acid on the surface, we performed computational modeling and explored possible mechanisms that could drive the shift in pK_a from solution to surface. Previous studies have suggested that the decreased dielectric on the surface could be a driving force.[41,42] Alternatively or in addition, the thiol deprotonation upon surface binding may have a similar effect on the carboxylic acid. However, our computational analysis showed that the charge density of the adsorbate molecule when bound to the surface as a thiolate is similar to the molecule with a protonated thiol for both models with and without solvent (Figures S29-S32 and Tables S6 and S7). Given these results, it appears unlikely that the shift in pK_a is a result of the thiol deprotonation upon surface binding and additionally that the thiol form might represent a reasonably simplified model for further computational analysis. We proceeded to calculate the predicted pK_a of a single molecule in water for both isomers. In both cases, the predicted pK_a was lower than what we observed experimentally in solution titrations with differences of 1.9 and 2.2 for **M1-COOH** and **M9-COOH**, respectively (Table S8).

To assess the effect of the dielectric on the surface, we first looked at the pK_a shift due to interactions between neighboring molecules, in the form of a dimer model (Figure S33). These calculations predicted increases in pK_a for both isomers with pK_a shifts from single-molecule to dimer configurations of 1.9 and 1.1 respectively for **M1-COOH** and **M9-COOH (**Table S9**).** These shifts are comparable to, but somewhat smaller than what we see experimentally between solution and surface pK_a, suggesting that molecular interactions within the monolayers play major roles in the differences between the unrestricted three-dimensional and surface-constrained two-dimensional environments, but that there may be other influencing factors. Additionally, for the shifts given above, the

molecular dimers were in configuration B as shown in Figure 4, with the carboxyl group positioned more laterally. We also modeled a dimer in configuration A for **M1-COOH**, which had a pK_a shift of only 0.1 from the free molecule. This model suggests that the characteristics of configuration A are similar to a free molecule in solution, further indicating that it is configuration B that is present on the surface for both isomers. We further calculated a range of pK_a *vs.* dielectric by modeling the molecule in different solvation fields for both **M1-COOH** and **M9-COOH** (Figure 6)**.** For both isomers, the modeling shows exponential trends that as dielectric decreases, pK_a increases. The corresponding dielectric based on the pK_a in the dimer configuration is 17 for **M1-COOH** and 25 for **M9-COOH**. Overall, our computational analyses suggest that the shift in pK_a is driven by the dielectric of the environment that the carboxyl group experiences on the surface. The interactions with neighboring molecules factor into this dielectric, but proximity to the Au surface and partial desolvation also make contributions. The computational model does take into account the effect of desolvation, but does not take into account the presence of the surface. However, given that the Au surface is separated from the carboxyl group by the molecular backbone, we believe that this model is a reasonable simulation of the surface environment.

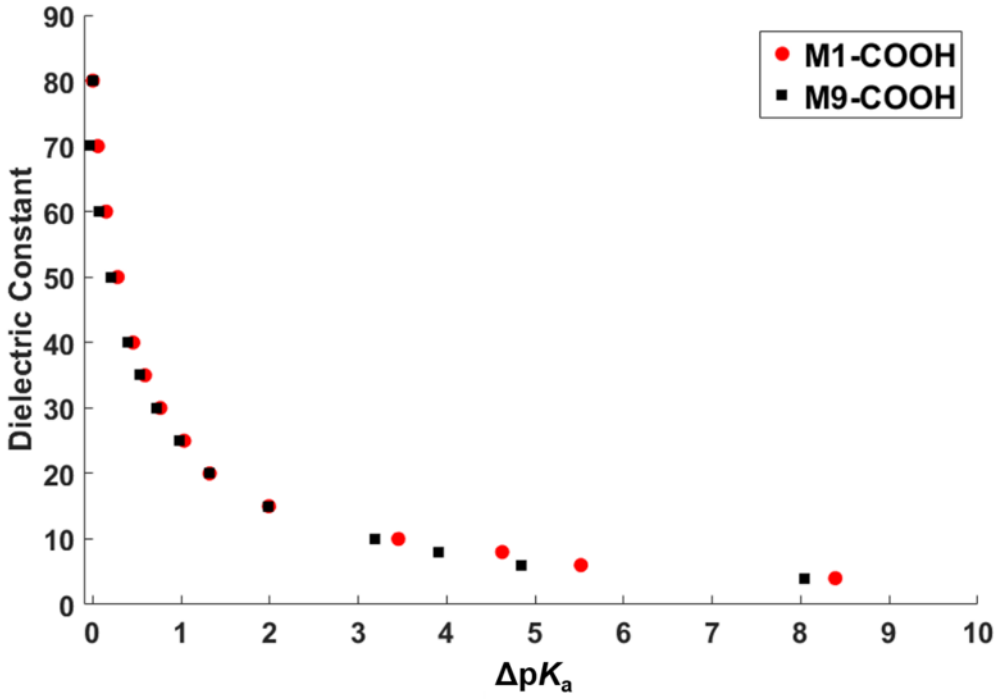

Figure 6. Computational results of the pK_a shift (ΔpK_a) in solvents with a range of dielectric constants for both isomers. The results show exponential relationships between the pK_a and the dielectric. Based on the pK_a calculated for the dimer configurations, the associated dielectrics are 17 and 25 for **M1-COOH** and **M9-COOH**, respectively.

Accessibility of carboxyl groups for surface-supported coordination chemistry was probed experimentally by examining the interactions between carboxyl-terminated SAMs and various ions.[43-45] The SAMs of the carboxylated isomers were exposed to dilute solutions of metal cations and the formation of metal coordination complexes was analyzed *via* XPS (summaries of the XPS investigations and the XPS spectra used for quantitative analysis are presented in the Supporting information, Tables S10-S12 and Figures S34 and S45). A total of 16 representative ions from across the periodic table were used, Na(I), Mg(II), Ca(II), Sr(II), Ba(II), Fe(II), Fe(III), Co(II), Ni(II), Cu(II), Zn(II), La(III), Sm(III),

Tb(III), Tl(I), and Pb(II). All of the ions interacted with the carboxyl-terminated SAMs and successfully replaced the intrinsically present Na(I) ions, which might originate from the solvents or glassware used for the preparation of the samples, as has been reported previously in literature[46] (detailed procedures for sample preparation for XPS are available in the Supporting information). Both starting SAMs of **M1-COOH** and **M9-COOH** were examined broadly; since the SAMs were found to have indistinguishable surface patterns and practically identical chemical behaviors, SAMs of **M9-COOH** were examined in greater detail. Also, SAMs of the **M9** isomer were used as control samples to test if the ions bind exclusively to the carboxylic moiety. The SAMs of **M9** were analyzed both before and after exposure to solutions of Na(I) and Mg(II) ions with no metal ions detected in those samples with XPS.

In addition, quantitative XPS analyses determining the metal ion/**M9-COOH** surface ratios for the pristine **M9-COOH** SAM and for the **M9-COOH** SAM modified with Mg(II) and Ba(II) ions, summarized in Table 5, indicate possible formation of bridging intermolecular surface complexes within the adsorbed monolayers, which is of interest due to its additional stabilizing effects.

Table 5. Measured ratios of the number of deposited metal ions to the number of **M9-COOH** molecules within the self-assembled monolayers (SAMs), together with the nominal kinetic energies of the photoelectrons used for the quantification of the metal ion (in parentheses).

SAM	Metal ion	Metal ion/**M9-COOH** ratio (binding energy used)
M9-COOH	Na	0.8 (415 eV)
M9-COOH + Mg(II)	Mg	0.3 (1180 eV), 0.5 (183 eV)
M9-COOH + Ba(II)	Ba	0.5 (706 eV)

Carboranethiol SAMs used in this study were labile under excess acidic conditions. Losses of surface coverage have been observed in XPS as the stoichiometries of the acidified monolayers exhibited higher content of the substrate gold when compared to the pristine SAMs, due to the removal of carboranethiol molecules (Table S11). Our previous investigations of SAMs of *para*-carboranedithiol, 1,12-$(SH)_2$-1,12-$C_2B_{10}H_{11}$ (**P1,12**), *para*-carboranethiol, 1-SH-1,12-$C_2B_{10}H_{11}$ (**P1**), and of its carboxylated derivative, 1-COOH-12-SH-1,12-$C_2B_{10}H_{10}$ (**P1-COOH**) showed that a fraction of molecules physisorbed as thiols and are thus more prone to desorption.[11,47] The thiol and thiolate species are easily distinguishable in XPS. The S 2p binding energies (BEs) of both free and adsorbed thiols are shifted by about +2 eV with respect to the corresponding thiolate forms (Figure 7). Desorption has been observed for all the samples subjected to relatively strong acidic environments, *i.e.*, SAMs of **M9** and **M9-COOH**, and **P1-COOH**, which have been

used as a comparison and also as a reference to our previous studies. The labile character of SH-bound carborane moieties makes them easy to wash from the surface and consequently leaving only the stronger thiolate-bound moieties and more of the bare gold surface exposed to XPS analysis. We assume that the anchoring thiolate group becomes protonated under acidic conditions, and the physisorbed thiol species are then easily washed away by rinsing in an excess of pure solvent,

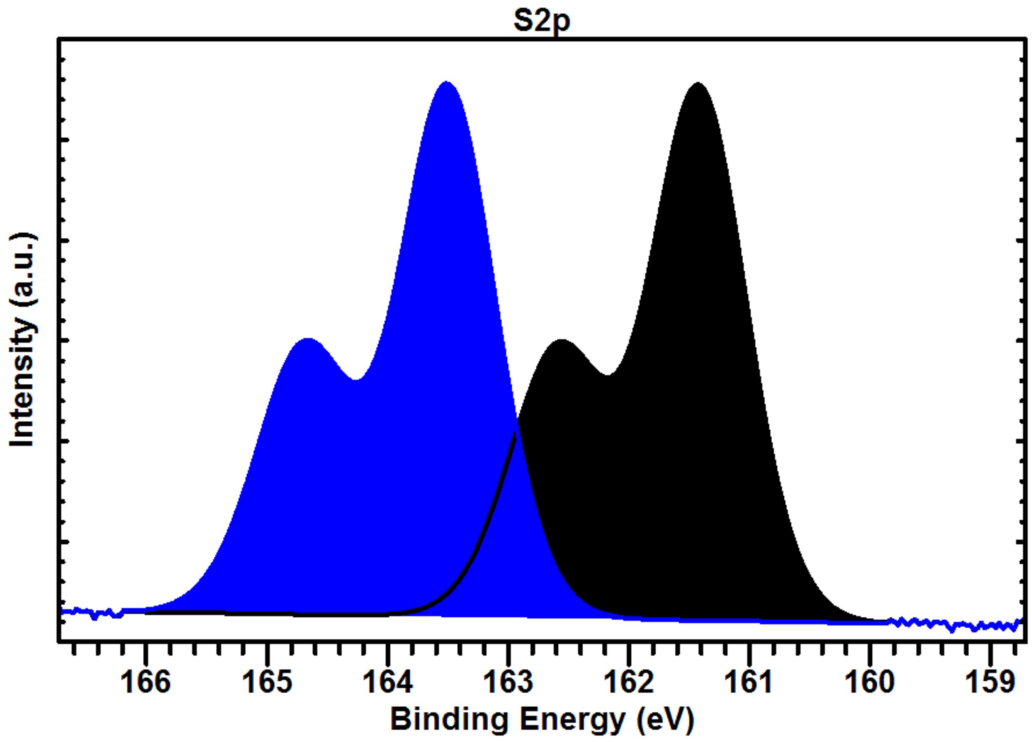

Figure 7. Approximate fit based on experimental X-ray photoelectron spectra showing the difference in the binding energies of S 2p doublets of thiolate (black) and thiol (blue) forms of **M9-COOH**. The illustration shows an overlay of the respective mono- and di-sodium salts of 1-carboxyl-9-mercapto-*meta*-carborane S 2p regions.

CONCLUSIONS AND PROSPECTS

Two new isomeric bifunctional cage molecules, derived from 12-vertex *m*-carborane, were synthesized and characterized using structural and spectroscopic methods. Both new building blocks for self-assembled monolayers on Au surfaces have greater steric demands compared to their parent non-carboxylated derivatives. The impact on the structural and chemical properties of these building blocks on the properties of their respective SAMs was investigated. These molecules represent systems that enable analyses of intramolecular communication between functional groups interspaced by *meta*-carborane skeletons. The effects of the carboxyl group are neither detected on the free thiol group in the ^{1}H NMR spectrum nor on the BE value of S $2p_{3/2}$ electrons upon surface adsorption. Both isomers show greater carboxyl group acidities compared to 1-COOH-*meta*-carborane reference, which are attributed to the effects of the thiol groups. This result is of general interest due to the *pseudo*-aromatic character of carboranes and their skeletal interactions with a wide range of functional groups. Although the molecules of both isomers exhibit different symmetries with one isomer being chiral, they arrange into identical hexagonal close-packed arrays on Au{111}. The greater steric demands of both isomers compared to their parent non-carboxylated molecules lead only to increases of the nearest neighbor spacings from 7.2 ± 0.4 Å to 8.4 ± 0.4 Å, relative to unfunctionalized carboranethiols, which is in good agreement with tilting the molecules 13-16° to minimize their lateral steric requirements and to maximize packing density. The addition of a lateral carboxyl group thus exerts a significant influence on the nearest neighbor spacings in the SAM. Analyses of the surface structure also suggest the presence of long-range

interactions, which could be due to a combination of hydrogen-bonding and favorable dipole-dipole interactions within the monolayer. The interactions of both isomeric molecules with gold surfaces were investigated by XPS, which shows that the molecules adsorb as thiolates. More detailed measurements show that the binding energies of S $2p_{3/2}$ electrons are influenced by electron-accepting and electron-donating properties of the carboranyl moiety. The assemblies also showed changes in the behavior of the carboxyl terminus at the environmental interface of the monolayer, resulting in pK_a shifts of ~2 pH units. Based on computational modeling, this shift appears to be a result of the dielectric of the environment that the carboxyl group experiences; this dielectric is determined by the interactions between neighboring molecules, proximity to the Au surface, and partial desolvation. The exposed surfaces of the SAMs are also accessible for several different types of ions to interact with the carboxylic group. These results show that the carboxyl-terminated *meta*-carborane building blocks open the monolayers to further interactions with different types of ions or molecules.

Understanding the influence on assembly and the reactivity of the carboxylic group in these carboranethiolate monolayers lays the groundwork for performing additional chemistry and developing further applications using the reactive interfaces. The tunable characteristics of carboranethiolate SAMs along with their pristine and essentially defect-free morphology make them advantageous for use in nanoscale and molecular devices.[23,48,49] These terminal carboxylic acids provide an avenue for fabricating three-dimensional heterostructures by facilitating such techniques as atomic layer deposition. Furthermore, given the acid-base reactivity of these SAMs there are also opportunities for their use in pH sensors.[11,50] The addition of a reactive platform to these

monolayers, combined with their already existing useful features, provides a foundation for both addressing fundamental chemistry questions and further applications, which would not be feasible with other systems.

Shifts in pK_a, similar to those we report on in this study, have been observed in protein systems and are linked to the dielectric of the microenvironment.[51-53] Our interest and detailed analysis of the surface-bound carboxyl functionalities and their respective chemical state and behavior is applicable to designing materials with adjustable and bio-responsive functions. To expand on this idea, amino acids in proteins experience multiple microenvironments and their pK_a values, along with the structure of the protein, adjust accordingly to facilitate function and catalysis.[51,54,55] These functionalized carboranethiolate monolayers serve as model platforms to study the driving forces relevant to pK_a changes in more complex biological and chemical systems.[55,56] Given the two-dimensional nature of these monolayers, they are particularly relevant for comparison to naturally occurring membrane-bound biological structures with constraints similar to those found in 2-dimensional self-organized arrays.

ASSOCIATED CONTENT

Supporting Information includes synthetic protocols, experimental and computational NMR data, mass spectrometry and infrared analyses, and single-crystal X-ray diffraction characterization data, STM experimental information, and additional STM images of the SAM-modified Au{111} surfaces. Also included are titration data in solution and on the SAM-modified Au{111} surfaces and XPS data of modified SAMs. Computational results

of surface conformations and surface acidity are provided. Files with the calculated atomic coordinates (xyz file formats) of both molecules and crystallographic information files are attached. This material is available free of charge via the Internet at http://pubs.acs.org.

AUTHOR INFORMATION

Corresponding Authors

*(P.S.W.) E-mail: psw@cnsi.ucla.edu

*(T.B.) E-mail: tbase@iic.cas.cz

*(A.N.A.) E-mail: ana@chem.ucla.edu

*(E.M.) E-mail: emete@balikesir.edu.tr

*(F.M.D.) E-mail: danisman@metu.edu.tr

*(K.N.H.) Email: houk@chem.ucla.edu

ORCID

Dominic P. Goronzy: 0000-0003-2856-4732

Jan Staněk: 0000-0002-7394-5035

Erin Avery: 0000-0002-6361-6967

Han Guo: 0000-0001-7695-9080

Zdeněk Bastl: 0000-0001-6857-4324

Michal Dušek: 0000-0001-9797-2559

Saliha Gün: 0000-0002-9613-1763

Brian J. Lewandowski: 0000-0002-8139-9417

Jan Macháček: 0000-0003-4723-0789

Václav Šícha: 0000-0003-3163-1764

John C. Thomas: 0000-0002-2151-7725

Adem Yavuz: 0000-0003-1086-3443

Kendall N. Houk: 0000-0002-8387-5261

Fatih M. Danisman: 0000-0002-7252-3113

Ersen Mete: 0000-0002-0916-5616

Anastassia N. Alexandrova: 0000-0002-3003-1911
Tomáš Baše: 0000-0003-2533-8705
Paul S. Weiss: 0000-0001-5527-6248

ACKNOWLEDGMENTS

This work was supported by the Ministry of Education, Youth and Sports of the Czech Republic (Program Inter-Excellence, subprogram Inter-Action), Grant no. LTAIN19152, the Technology Agency of the Czech Republic, Grant no. TH02020628, the Scientific and Technological Research Council of Turkey (TUBITAK) Grant No. 116F174, Middle East Technical University Grant No. YLT-103-2018-3684, and the US Department of Energy Grant No. DE-SC-0005161. A.N.A. acknowledges US Department of Energy Grant No. DE-SC-0019245. Access to the computing and storage facilities owned by parties and projects contributing to the National Grid Infrastructure MetaCentrum, provided under the programme "Projects of Large Research, Development, and Innovations Infrastructures" (CESNET LM2015042), is greatly appreciated. The authors are thankful for the support of Prof. Jiří Vohlídal from Charles University in Prague. XPS part of the work was done with the support of CEITEC Nano Research Infrastructure (ID LM2015041, MEYS CR, 2016–2019). Single-crystal X-ray diffraction analysis was done within the Czech Science Foundation project no. 18-10438S. T.B. and P.S.W. thank the Fulbright Commission for their support of the project “Dipole-Dipole Interactions in Self-Assembled Materials”.

REFERENCES

1. Love, J. C.; Estroff, L. A.; Kriebel, J. K.; Nuzzo, R. G.; Whitesides, G. M. Self-Assembled Monolayers of Thiolates on Metals as a Form of Nanotechnology. *Chem. Rev.* **2005,** *105*, 1103-1170.
2. Vericat, C.; Vela, M. E.; Benitez, G.; Carro, P.; Salvarezza, R. C. Self-Assembled Monolayers of Thiols and Dithiols on Gold: New Challenges for a Well-Known System. *Chem. Soc. Rev.* **2010,** *39*, 1805.
3. Claridge, S. A.; Liao, W.-S.; Thomas, J. C.; Zhao, Y.; Cao, H. H.; Cheunkar, S.; Serino, A. C.; Andrews, A. M.; Weiss, P. S. From the Bottom Up: Dimensional Control and Characterization in Molecular Monolayers. *Chem. Soc. Rev.* **2013,** *42*, 2725-2745.
4. Goronzy, D. P.; Ebrahimi, M.; Rosei, F.; Arramel; Fang, Y.; De Feyter, S.; Tait, S. L.; Wang, C.; Beton, P. H.; Wee, A. T. S.; Weiss, P. S.; Perepichka, D. F. Supramolecular Assemblies on Surfaces: Nanopatterning, Functionality, and Reactivity. *ACS Nano* **2018,** *12*, 7445-7481.
5. Hohman, J. N.; Claridge, S. A.; Kim, M.; Weiss, P. S. Cage Molecules for Self-Assembly. *Mater. Sci. Eng., R* **2010,** *70*, 188-208.
6. Laibinis, P. E.; Whitesides, G. M. Ω-Terminated Alkanethiolate Monolayers on Surfaces of Copper, Silver, and Gold Have Similar Wettabilities. *J. Am. Chem. Soc.* **1992,** *114*, 1990-1995.
7. Gershevitz, O.; Osnis, A.; Sukenik, C. N. Interfacial Chemistry on Carboxylate-Functionalized Monolayer Assemblies. *Isr. J. Chem.* **2005,** *45*, 321-336.
8. Burris, S. C.; Zhou, Y.; Maupin, W. A.; Ebelhar, A. J.; Daugherty, M. W. The Effect of Surface Preparation on Apparent Surface pK_a's of Ω-Mercaptocarboxylic Acid Self-Assembled Monolayers on Polycrystalline Gold. *J. Phys. Chem. C* **2008,** *112*, 6811-6815.
9. Hirata, N.; Suga, S.; Noguchi, Y.; Shibuta, M.; Tsunoyama, H.; Eguchi, T.; Nakajima, A. Highly Ordered Self-Assembled Monolayers of Carboxy- and Ester-Terminated Alkanethiols on Au(111): Infrared Absorption and Hyperthermal-Deposition Experiments with Cr(benzene)$_2$ Ions. *J. Phys. Chem. C* **2017,** *121*, 6736-6747.
10. Ackerson, C. J.; Jadzinsky, P. D.; Kornberg, R. D. Thiolate Ligands for Synthesis of Water-Soluble Gold Clusters. *J. Am. Chem. Soc.* **2005,** *127*, 6550-6551.
11. Thomas, J. C.; Boldog, I.; Auluck, H. S.; Bereciartua, P. J.; Dušek, M.; Macháček, J.; Bastl, Z.; Weiss, P. S.; Baše, T. Self-Assembled *p*-Carborane Analogue of *p*-Mercaptobenzoic Acid on Au{111}. *Chem. Mater.* **2015,** *27*, 5425-5435.
12. Hohman, J. N.; Zhang, P.; Morin, E. I.; Han, P.; Kim, M.; Kurland, A. R.; McClanahan, P. D.; Balema, V. P.; Weiss, P. S. Self-Assembly of Carboranethiol Isomers on Au{111}: Intermolecular Interactions Determined by Molecular Dipole Orientations. *ACS Nano* **2009,** *3*, 527-536.
13. Kim, M.; Hohman, J. N.; Morin, E. I.; Daniel, T. A.; Weiss, P. S. Self-Assembled Monolayers of 2-Adamantanethiol on Au{111}: Control of Structure and Displacement. *J. Phys. Chem. A* **2009,** *113*, 3895-3903.
14. Fujii, S.; Akiba, U.; Fujihira, M. Geometry for Self-Assembling of Spherical Hydrocarbon Cages with Methane Thiolates on Au(111). *J. Am. Chem. Soc.* **2002,** *124*, 13629-13635.

15. Dameron, A. A.; Charles, L. F.; Weiss, P. S. Structures and Displacement of 1-Adamantanethiol Self-Assembled Monolayers on Au{111}. *J. Am. Chem. Soc.* **2005,** *127*, 8697-8704.
16. Willey, T. M.; Fabbri, J. D.; Lee, J. R. I.; Schreiner, P. R.; Fokin, A. A.; Tkachenko, B. A.; Fokina, N. A.; Dahl, J. E. P.; Carlson, R. M. K.; Vance, A. L.; Yang, W.; Terminello, L. J.; Buuren, T. v.; Melosh, N. A. Near-Edge X-Ray Absorption Fine Structure Spectroscopy of Diamondoid Thiol Monolayers on Gold. *J. Am. Chem. Soc.* **2008,** *130*, 10536-10544.
17. Baše, T.; Bastl, Z.; Plzák, Z.; Grygar, T.; Plešek, J.; Carr, M. J.; Malina, V.; Šubrt, J.; Boháček, J.; Večerníková, E.; Kříž, O. Carboranethiol-Modified Gold Surfaces. A Study and Comparison of Modified Cluster and Flat Surfaces. *Langmuir* **2005,** *21*, 7776-7785.
18. Grimes, R. N. Carboranes in the Chemist's Toolbox. *Dalton Trans.* **2015,** *44*, 5939-5956.
19. Spokoyny, A. M.; Machan, C. W.; Clingerman, D. J.; Rosen, M. S.; Wiester, M. J.; Kennedy, R. D.; Stern, C. L.; Sarjeant, A. A.; Mirkin, C. A. A Coordination Chemistry Dichotomy for Icosahedral Carborane-Based Ligands. *Nature Chemistry* **2011,** *3*, 590-596.
20. Yavuz, A.; Sohrabnia, N.; Yilmaz, A.; Danışman, M. F. Mixed Carboranethiol Self-Assembled Monolayers on Gold Surfaces. *Appl. Surf. Sci.* **2017,** *413*, 233-241.
21. Lübben, J. F.; Baše, T.; Rupper, P.; Künniger, T.; Macháček, J.; Guimond, S. Tuning the Surface Potential of Ag Surfaces by Chemisorption of Oppositely-Oriented Thiolated Carborane Dipoles. *J. Colloid Interface Sci.* **2011,** *354*, 168-174.
22. Thomas, J. C.; Schwartz, J. J.; Hohman, J. N.; Claridge, S. A.; Auluck, H. S.; Serino, A. C.; Spokoyny, A. M.; Tran, G.; Kelly, K. F.; Mirkin, C. A.; Gilles, J.; Osher, S. J.; Weiss, P. S. Defect-Tolerant Aligned Dipoles within Two-Dimensional Plastic Lattices. *ACS Nano* **2015,** *9*, 4734-4742.
23. Kim, J.; Rim, Y. S.; Liu, Y.; Serino, A. C.; Thomas, J. C.; Chen, H.; Yang, Y.; Weiss, P. S. Interface Control in Organic Electronics Using Mixed Monolayers of Carboranethiol Isomers. *Nano Lett.* **2014,** *14*, 2946-2951.
24. Vetushka, A.; Bernard, L.; Guseva, O.; Bastl, Z.; Plocek, J.; Tomandl, I.; Fejfar, A.; Baše, T.; Schmutz, P. Adsorption of Oriented Carborane Dipoles on a Silver Surface. *Phys. Status Solidi B* **2015,** *253*, 591-600.
25. Mete, E.; Yılmaz, A.; Danışman, M. F. A van der Waals Density Functional Investigation of Carboranethiol Self-Assembled Monolayers on Au(111). *Phys. Chem. Chem. Phys.* **2016,** *18*, 12920-12927.
26. Plešek, J. The Age of Chiral Deltahedral Borane Derivatives. *Inorg. Chim. Acta* **1999,** *289*, 45-50.
27. Abendroth, J. M.; Stemer, D. M.; Bloom, B. P.; Roy, P.; Naaman, R.; Waldeck, D. H.; Weiss, P. S.; Mondal, P. C. Spin Selectivity in Photoinduced Charge-Transfer Mediated by Chiral Molecules. *ACS Nano* **2019,** *13*, 4928-4946.
28. Gohler, B.; Hamelbeck, V.; Markus, T. Z.; Kettner, M.; Hanne, G. F.; Vager, Z.; Naaman, R.; Zacharias, H. Spin Selectivity in Electron Transmission through Self-Assembled Monolayers of Double-Stranded DNA. *Science* **2011,** *331*, 894-897.
29. Abendroth, J. M.; Nakatsuka, N.; Ye, M.; Kim, D.; Fullerton, E. E.; Andrews, A. M.; Weiss, P. S. Analyzing Spin Selectivity in DNA-Mediated Charge Transfer *via* Fluorescence Microscopy. *ACS Nano* **2017,** *11*, 7516-7526.

30. Abendroth, J. M.; Cheung, K. M.; Stemer, D. M.; El Hadri, M. S.; Zhao, C.; Fullerton, E. E.; Weiss, P. S. Spin-Dependent Ionization of Chiral Molecular Films. *J. Am. Chem. Soc.* **2019,** *141*, 3863-3874.
31. Bregadze, V. I. Dicarba-*Closo*-Dodecaboranes $C_2B_{10}H_{12}$ and Their Derivatives. *Chem. Rev.* **1992,** *92*, 209-223.
32. Plešek, J.; Heřmánek, S. Experimental Evaluation of Charge Distribution on Particular Skeletal Atoms in Icosahedral Carboranes by Means of HS-Derivatives. *Collect. Czech. Chem. Commun.* **1979,** *44*, 24-33.
33. Plešek, J.; Heřmánek, S. Syntheses and Properties of Substituted Icosahedral Carborane Thiols. *Collect. Czech. Chem. Commun.* **1981,** *46*, 687-692.
34. Grimes, R. N. Carboranes, 3rd Edition. Elsevier: 2016.
35. Baše, T.; Macháček, J.; Hájková, Z.; Langecker, J.; Kennedy, J. D.; Carr, M. J. Thermal Isomerizations of Monothiolated Carboranes $(HS)C_2B_{10}H_{11}$ and the Solid-State Investigation of 9-(HS)-1,2-$C_2B_{10}H_{11}$ and 9-(HS)-1,7-$C_2B_{10}H_{11}$. *J. Organomet. Chem.* **2015,** *798*, 132-140.
36. Thomas, J. C.; Goronzy, D. P.; Dragomiretskiy, K.; Zosso, D.; Gilles, J.; Osher, S. J.; Bertozzi, A. L.; Weiss, P. S. Mapping Buried Hydrogen-Bonding Networks. *ACS Nano* **2016,** *10*, 5446-5451.
37. Maksymovych, P.; Sorescu, D. C.; Yates, J. T. Gold-Adatom-Mediated Bonding in Self-Assembled Short-Chain Alkanethiolate Species on the Au(111) Surface. *Phys. Rev. Lett.* **2006,** *97*, 146103.
38. Moore, A. M.; Mantooth, B. A.; Donhauser, Z. J.; Yao, Y.; Tour, J. M.; Weiss, P. S. Real-Time Measurements of Conductance Switching and Motion of Single Oligo(Phenylene Ethynylene) Molecules. *J. Am. Chem. Soc.* **2007,** *129*, 10352-10353.
39. Hohman, J. N.; Kim, M.; Schüpbach, B.; Kind, M.; Thomas, J. C.; Terfort, A.; Weiss, P. S. Dynamic Double Lattice of 1-Adamantaneselenolate Self-Assembled Monolayers on Au{111}. *J. Am. Chem. Soc.* **2011,** *133*, 19422-19431.
40. Bain, C. D.; Whitesides, G. M. A Study by Contact Angle of the Acid-Base Behavior of Monolayers Containing Ω-Mercaptocarboxylic Acids Adsorbed on Gold: An Example of Reactive Spreading. *Langmuir* **1989,** *5*, 1370-1378.
41. Creager, S. E.; Clarke, J. Contact-Angle Titrations of Mixed Ω-Mercaptoalkanoic Acid/Alkanethiol Monolayers on Gold. Reactive vs Nonreactive Spreading, and Chain Length Effects on Surface pK_a Values. *Langmuir* **1994,** *10*, 3675-3683.
42. Paulo, T. F.; Abruña, H. D.; Diógenes, I. C. N. Thermodynamic, Kinetic, Surface pK_a, and Structural Aspects of Self-Assembled Monolayers of Thio Compounds on Gold. *Langmuir* **2012,** *28*, 17825-17831.
43. Hatzor, A.; Weiss, P. S. Molecular Rulers for Scaling Down Nanostructures. *Science* **2001,** *291*, 1019.
44. Mandal, S.; Reber, A. C.; Qian, M.; Weiss, P. S.; Khanna, S. N.; Sen, A. Controlling the Band Gap Energy of Cluster-Assembled Materials. *Acc. Chem. Res.* **2013,** *46*, 2385-2395.
45. Andrews, A. M.; Liao, W.-S.; Weiss, P. S. Double-Sided Opportunities Using Chemical Lift-Off Lithography. *Acc. Chem. Res.* **2016,** *49*, 1449-1457.
46. Arnold, R.; Azzam, W.; Terfort, A.; Wöll, C. Preparation, Modification, and Crystallinity of Aliphatic and Aromatic Carboxylic Acid Terminated Self-Assembled Monolayers. *Langmuir* **2002,** *18*, 3980-3992.

47. Baše, T.; Bastl, Z.; Šlouf, M.; Klementová, M.; Šubrt, J.; Vetushka, A.; Ledinský, M.; Fejfar, A.; Macháček, J.; Carr, M. J.; Londesborough, M. G. S. Gold Micrometer Crystals Modified with Carboranethiol Derivatives. *J. Phys. Chem. C* **2008,** *112*, 14446-14455.
48. Schwartz, J. J.; Mendoza, A. M.; Wattanatorn, N.; Zhao, Y.; Nguyen, V. T.; Spokoyny, A. M.; Mirkin, C. A.; Baše, T.; Weiss, P. S. Surface Dipole Control of Liquid Crystal Alignment. *J. Am. Chem. Soc.* **2016,** *138*, 5957-5967.
49. Serino, A. C.; Anderson, M. E.; Saleh, L. M. A.; Dziedzic, R. M.; Mills, H.; Heidenreich, L. K.; Spokoyny, A. M.; Weiss, P. S. Work Function Control of Germanium through Carborane-Carboxylic Acid Surface Passivation. *ACS Appl. Mater. Interfaces* **2017,** *9*, 34592-34596.
50. Thomas, J. C.; Goronzy, D. P.; Serino, A. C.; Auluck, H. S.; Irving, O. R.; Jimenez-Izal, E.; Deirmenjian, J. M.; Macháček, J.; Sautet, P.; Alexandrova, A. N.; Baše, T.; Weiss, P. S. Acid–Base Control of Valency within Carboranedithiol Self-Assembled Monolayers: Molecules Do the Can-Can. *ACS Nano* **2018,** *12*, 2211-2221.
51. Isom, D. G.; Castañeda, C. A.; Cannon, B. R.; García-Moreno E, B. Large Shifts in pK_a Values of Lysine Residues Buried inside a Protein. *Proc. Natl. Acad. Sci. U. S. A.* **2011,** *108*, 5260.
52. Harms, M. J.; Castañeda, C. A.; Schlessman, J. L.; Sue, G. R.; Isom, D. G.; Cannon, B. R.; García-Moreno E, B. The pK_a Values of Acidic and Basic Residues Buried at the Same Internal Location in a Protein Are Governed by Different Factors. *J. Mol. Biol.* **2009,** *389*, 34-47.
53. Karp, D. A.; Gittis, A. G.; Stahley, M. R.; Fitch, C. A.; Stites, W. E.; García-Moreno E, B. High Apparent Dielectric Constant inside a Protein Reflects Structural Reorganization Coupled to the Ionization of an Internal Asp. *Biophys. J.* **2007,** *92*, 2041-2053.
54. Rastogi, V. K.; Girvin, M. E. Structural Changes Linked to Proton Translocation by Subunit *C* of the ATP Synthase. *Nature* **1999,** *402*, 263-268.
55. Guo, B.; Middha, E.; Liu, B. Solvent Magic for Organic Particles. *ACS Nano* **2019,** *13*, 2675-2680.
56. Chen, H.; Huang, C.; Deng, Y.; Sun, Q.; Zhang, Q.-L.; Zhu, B.-X.; Ni, X.-L. Solvent-Switched Schiff-Base Macrocycles: Self-Sorting and Self-Assembly-Dependent Unconventional Organic Particles. *ACS Nano* **2019,** *13*, 2840-2848.

For Table of Contents Only